International Journal of Fluid Machinery and Systems
Vol. 4, No. 2, April-June 2011

DOI: 10.5293/IJFMS.2011.4.2.262
ISSN (Online): 1882-9554

Original Paper

Vortices within a Three-Dimensional Separation in an Axial Flow Stator of a Diagonal Flow Fan

Yoichi Kinoue[1], Norimasa Shiomi[1] and Toshiaki Setoguchi[2]

[1]Department of Mechanical Engineering, Saga University
1, Honjo, Saga, 840-8502, Japan, kinoue@me.saga-u.ac.jp
[2]Institute of Ocean Energy, Saga University
1, Honjo, Saga, 840-8502, Japan, setoguci@me.saga-u.ac.jp

Abstract

Experimental and numerical investigations were conducted for an internal flow in an axial flow stator of a diagonal flow fan. A corner separation near the hub surface and the suction surface of a stator blade was focused on, and further, three-dimensional vortices in separated flow were investigated by the numerical analysis. At low flow rate of 80% of the design flow rate, a corner separation of the stator between the suction surface and the hub surface can be found in both experimental and calculated results. Separation vortices are observed in the limiting streamline patterns both on the blade suction and on the hub surfaces at 80% of the design flow rate in the calculated results. It also can be observed in the streamline pattern that both vortices from the blade suction surface and from the hub surface keep vortex structures up to far locations from these wall surfaces. An attempt to explain the vortices within a three-dimensional separation is introduced by using vortex filaments.

Keywords: Diagonal flow fan, Axial flow stator, Internal flow, Corner separation, Five-hole probe survey, CFD

1. Introduction

In the case of high loading or partial flow rate of an axial compressor stator flow, a separated region exists in the corner between the blade suction surface and the hub wall as shown in Fig. 1, which is so called a corner stall or a corner separation. Flow in Fig. 1 is from right to left, and LE and TE mean the leading and the trailing edges. That kind of flow is highly three-dimensional viscous flow, which has a profound influence on the performance of blade rows.

Several studies concerning the three-dimensional separated flow in an axial compressor stator have been reported. Joslyn and Dring [1] investigated the flow in a stator with high loading and low aspect ratio. A stalled region with high aerodynamic loss in the corner of the suction surface and the hub wall was reported. Dong et al. [2] investigated flow and loss mechanism in a single-stage low-speed axial compressor stator. Large separated areas were observed at both near the hub and near the casing. Schulz and Gallus [3] performed detailed flow measurement in an isolated subsonic axial compressor stator at various blade loading. Blade wall and endwall visualizations, blade boundary layer investigations with hot wires and hot films, and five-hole probe measurements were done at stator outlet. Corner separations both near the hub and near the casing were observed for some case. On the other hand, Hah and Loelbach [4] performed the steady RANS analysis and incorporated their calculated results and the experimental results of Schulz and Gallus [3] in order to advance the understanding of the basic mechanism of compressor hub corner stall. A twisterlike vortex was observed near the rear part of the stator blade suction surface. Recently, Gbadebo et al. [5] have reported three-dimensional separation of stator cascade in terms of both topological and engineering considerations.

The main purpose of this study is to investigate the separated flow of rear stator cascade in the diagonal flow fan both experimentally and numerically, which can be considered as similar to an axial compressor stator flow. In the previous paper of the authors [6], the experimental results of the internal flows of both the axial flow stator and the diagonal flow rotor were reported. In this paper, a corner separation near the hub surface and the suction surface of the stator blade is especially focused on. Vortex structure in the three-dimensional separation was investigated in the numerical simulation.

Received December 8 2010; revised January 14 2011; accepted for publication January 27 2011: Review conducted by Prof. Yutaka Ota. (Paper number O10037J)
Corresponding author: Yoichi Kinoue, Associate Professor, kinoue@me.saga-u.ac.jp

Table 1 Specification of fan

Rotational speed		3100[min -1]
Design total pressure coefficient		0.345
Design flow rate coefficient		0.345
Type number		3.10
Duct diameter		380[mm]
Vortex pattern		Free vortex
Hub ratio		0.6
Inclination angle of hub		40[deg]
Inclination angle of casing		20[deg]
Rotor	Number of blade	6
	Max blade thickness chord length rate	Tip 5% Hub 10%
	Blade profile	NACA65
Stator	Number of blade	11
	Max blade thickness chord length rate	1%
	Blade profile	Circular arc blade

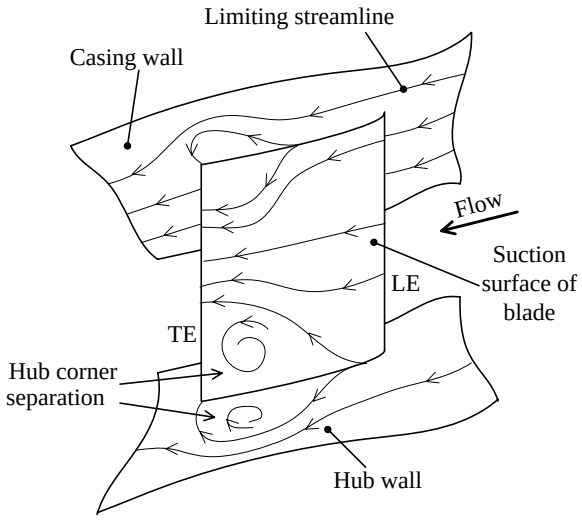

Fig. 1 Hub corner separation of stator

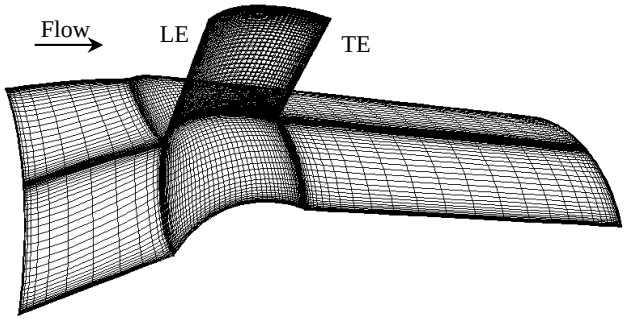

Fig. 4 Perspective view of grids

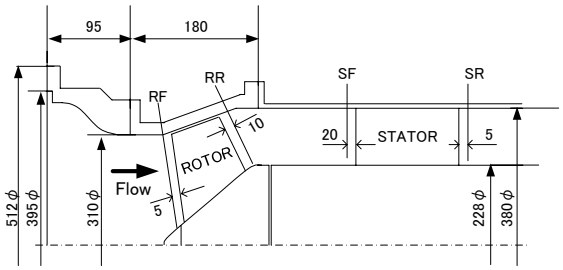

Fig. 2 Test section

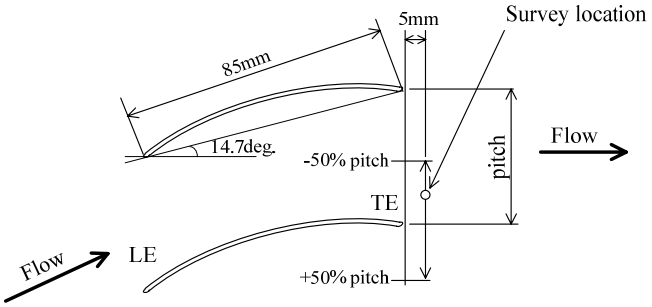

Fig. 3 Survey location at the back of stator

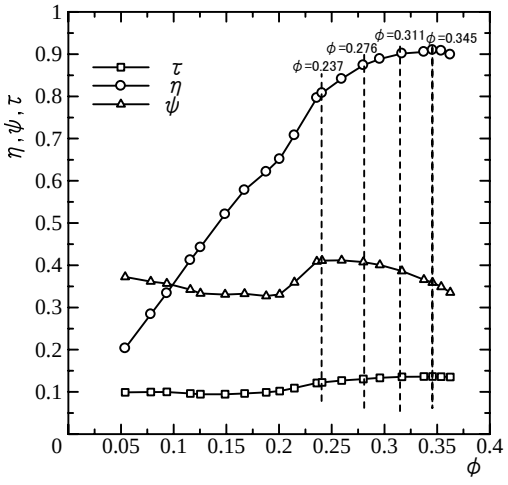

Fig. 5 Stage performance test

2. Experimental Apparatus and Procedure

The experimental apparatus in Saga University was used to investigate a stage performance of a diagonal flow fan [6]. By using this apparatus, the stage performance was evaluated as a combination of the rotor and the stator. The total pressure-rise of the stage was obtained from the pressure difference between the inlet chamber and the pressure tap which locates upstream of the damper. The torque was measured using a torque meter mounted on rotor shaft. The test Reynolds number is about 4.39×10^5 based on the blade chord length at mid-span and blade tip speed at leading edge.

Table 1 shows the specification of fan tested. The rotor comprises 6 blades designed by the use of a quasi three-dimensional method based on two-dimensional NACA65 cascade data. The stator comprises 11 blades, of which the blade element selection was carried out by using two-dimensional cascade data of circular-arc blade. The tip clearance of rotor is 0.5 mm and the clearance between the stator and the casing is 1.0 mm, which means that the stator is cantilevered by the hub wall.

Figure 2 shows the test section of the apparatus. The measurement of internal flow of the stator was conducted by using five-hole probe which is calibrated in advance. By using this probe, time-averaged values such as velocity vector and total pressure were measured. The axial location of measurement for stator was 20 mm upstream and 5 mm downstream of the leading edge and trailing edge, respectively. Fig. 3 shows the survey location at the back of stator. The circumferential survey locations at stator outlet were set from -50 % to +50 % in the pitchwise direction, where the minus sign means suction surface side and the plus sign means pressure surface side, respectively.

3. Numerical Analysis

Steady, three-dimensional Navier-Stokes numerical simulations were conducted for the flow field around a stator cascade. A commercial code, FLUENT6 was used in the numerical analysis. The steady, three-dimensional, Reynolds-averaged Navier-Stokes equations were discretized by the finite volume method in a strong conservation form. SIMPLE algorithm for incompressible flow was used to calculate velocity and pressure. The absolute coordinate for the stator was used. The second order accuracy upwind difference scheme was used for the convection term. The RNG k-ε turbulence model was used to calculate eddy viscosity.

The computation domain was extended 155 mm upstream from the leading edge and 310 mm downstream from the trailing edge, respectively. Fig. 4 shows the perspective view of grids for two-pitch calculation. The structured, hexahedral grids of H-type were used. The total number of the grids is approximately 700,000. No tip clearance is considered.

No slip condition was used for all wall surfaces. Periodic boundary conditions were used for the surfaces of circumferential side. On the upstream boundary, experimentally measured velocities by the five-hole probe survey were used. On the downstream boundary, the atmospheric pressure for static pressure was given.

For the pressure boundary condition, there is a difference between the experiment and the calculation. A stagnation pressure upstream of the test section is the atmospheric pressure in the experiment, whereas the downstream boundary pressure is the atmospheric pressure in the calculation. Even though there is a difference of pressure boundary, experimental and calculated values can be compared because pressure gradients are physically same between experiment and calculation in the incompressible flow.

Grid independency was checked by the calculation in which the total number of the grids is approximately 950,000. Velocities and pressures at the exit of stator flow, limiting streamlines along the surfaces of the blade suction and the hub were almost the same as the one for the 700,000 grids. The maximum value of y^+ along the blade surface for the 700,000 grids was about 10.

4. Results and Discussions

4.1 Stage Performance Test

Figure 5 shows the characteristic curves of the test fan. Total pressure efficiency η, total pressure-rise coefficient ψ and torque coefficient τ are plotted against flow-rate coefficient ϕ. These values are defined as follows.

$$\phi = Q/\left(AU^*\right) \tag{1}$$

$$\psi = \Delta P/\left(\rho U^{*2}/2\right) \tag{2}$$

$$\tau = T\omega/\left(\rho U^{*3} A/2\right) \tag{3}$$

$$\eta = \phi\psi/\tau \tag{4}$$

Where, $A=\pi\,(D_c^2-D_h^2)/4$ and U^* is the reference velocity, that is, $U^*=D_c\omega/2$.

Experimental value of ψ at design flow rate coefficient ϕ=0.345 agrees well with the design value ψ=0.345. Experimental value of η at ϕ=0.345 takes η =90.3 %. The value of ψ takes maximum at around ϕ=0.25. The internal flow measurement of stator were done by using five-hole probe at ϕ=0.345 (ϕ_{design}), ϕ=0.311 (0.9 ϕ_{design}) and ϕ =0.276 (0.8 ϕ_{design}), respectively. Further, three-dimensional Navier-Stokes numerical analysis was conducted at ϕ=0.345 (ϕ_{design}), ϕ=0.311 (0.9 ϕ_{design}) and ϕ =0.276 (0.8 ϕ_{design}), respectively.

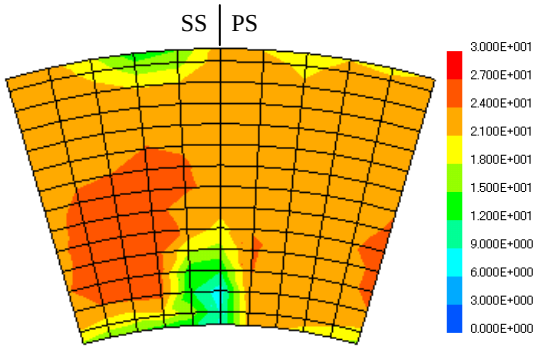

(a) $\phi = 0.345$ (ϕ_{design})

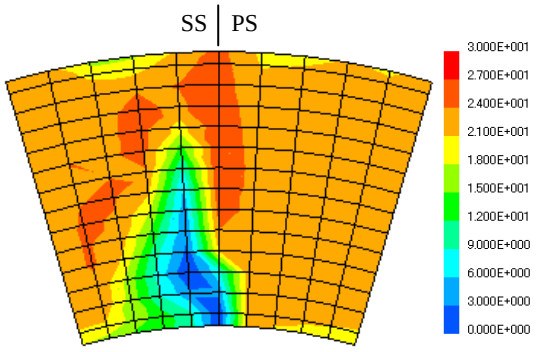

(b) $\phi = 0.311$ ($0.9\phi_{design}$)

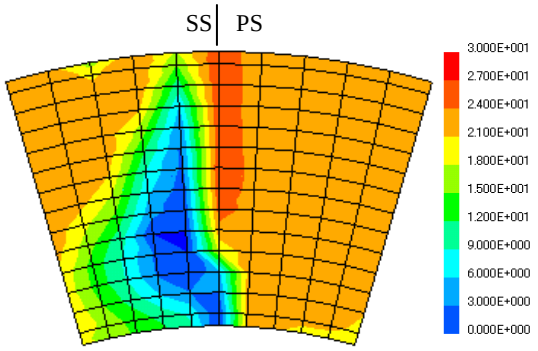

(c) $\phi = 0.276$ ($0.8\phi_{design}$)

Fig. 6 Experimental results of v_a at stator exit (unit: m/s)

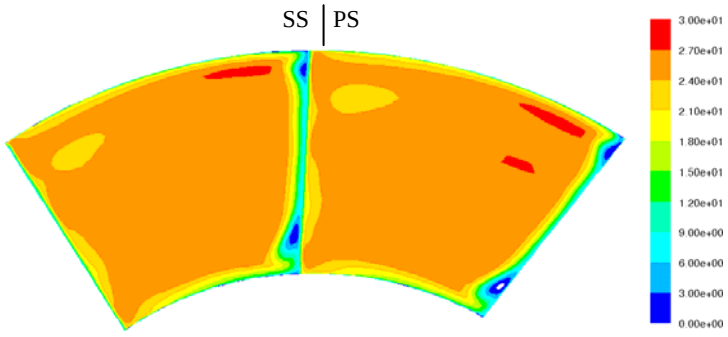

(a) $\phi = 0.345$ (ϕ_{design})

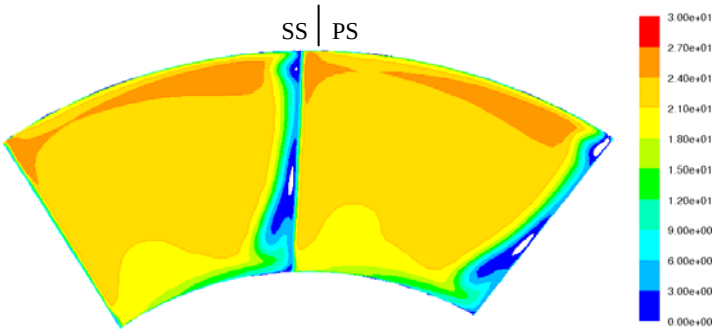

(b) $\phi = 0.311$ ($0.9\phi_{design}$)

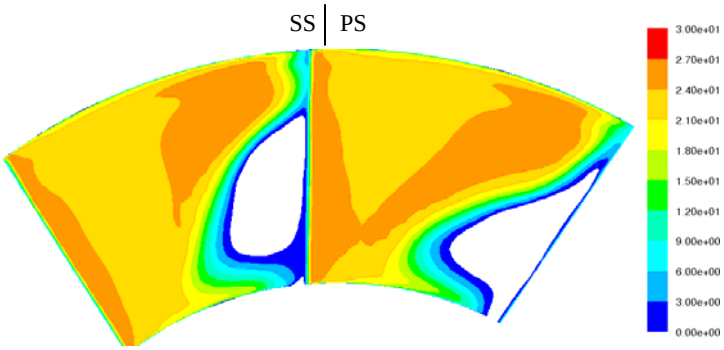

(c) $\phi = 0.276$ ($0.8\phi_{design}$)

Fig. 7 Calculated results of v_a at stator exit (unit: m/s)

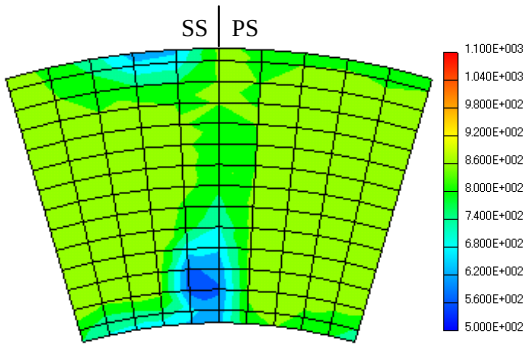

(a) $\phi = 0.345$ (ϕ_{design})

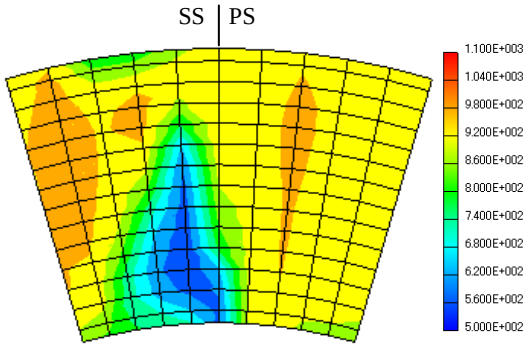

(b) $\phi = 0.311$ ($0.9\phi_{design}$)

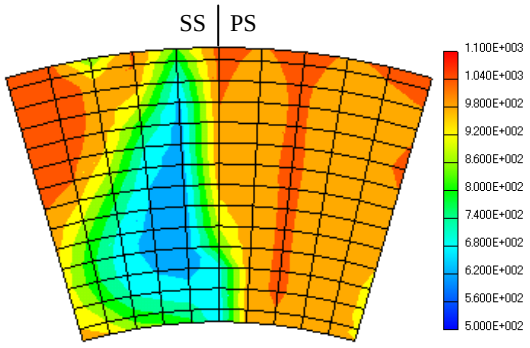

(c) $\phi = 0.276$ ($0.8\phi_{design}$)

Fig. 8 Experimental results of P_t at stator exit (unit: m/s)

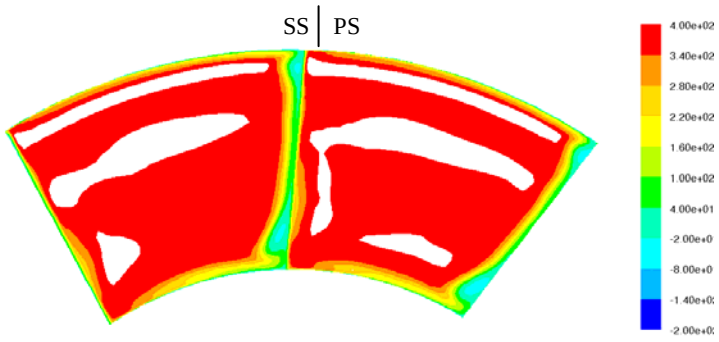

(a) $\phi = 0.345$ (ϕ_{design})

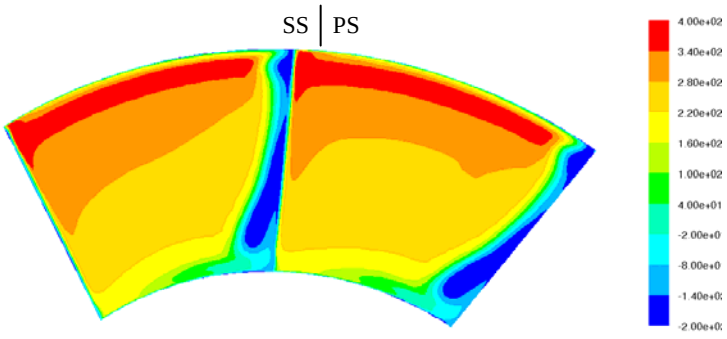

(b) $\phi = 0.311$ ($0.9\phi_{design}$)

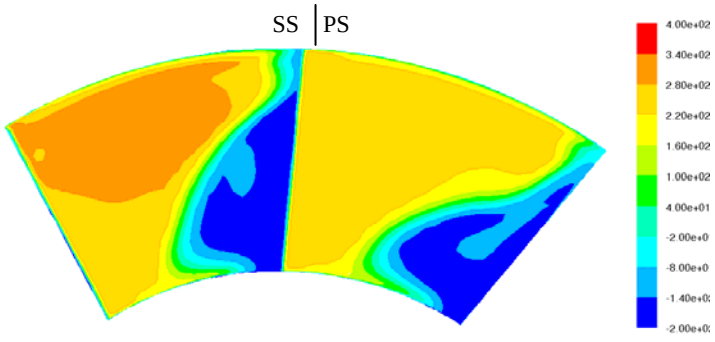

(c) $\phi = 0.276$ ($0.8\phi_{design}$)

Fig. 9 Calculated results of P_t at stator exit (unit: m/s)

In this paper, the three-dimensional calculation for the internal flow of stator blade of the diagonal fan stage was conducted. In order to compare the values of stage performance between the calculation and the experiment, further numerical investigations for the internal flow of rotor are needed.

4.2 Internal Flow Field

Figure 6 and Fig.7 show the contour maps of axial velocity v_a (time-averaged value) at stator exit, where Fig.6 shows the experimental results and Fig.7 shows the calculated results, and Fig.6(a) and Fig.7(a) show the results at design flow rate ϕ=0.345 (ϕ_{design}), Fig.6(b) and Fig.7(b) show the results at 90% of design flow rate ϕ=0.311 (0.9ϕ_{design}) and Fig.6(c) and Fig.7(c) show the results at 80% of design flow rate ϕ=0.276 (0.8ϕ_{design}), respectively. Also, Fig.8 and Fig.9 show the contour maps of total pressure P_t (time-averaged value) at stator exit by the same way as Fig.6 and Fig.7. In each contour map, thin solid lines show the location of trailing edge of the stator blade and the left side is the suction surface side (SS) and the right side is the pressure surface side (PS).

The maximum and minimum values of v_a are set as 0 and 30 m/s both in the experiment of Fig.6 and in the calculation of Fig.7. On the other hand, the maximum and minimum values of P_t in the calculation of Fig.9 are different from the ones in the experiment of Fig.8. This is because the absolute values of pressure in the calculation depend on the value of pressure on the downstream boundary. Only the pressure difference of each contour line has physical meaning, therefore, the difference between the maximum and minimum values of P_t in the calculation of Fig.9 is set as 600 Pa, which is the same as the value in the experiment of Fig.8. Blank areas in Fig.7 mean that the values of v_a are under 0 m/s and blank areas in Fig.9 mean that the values of P_t are over 400 Pa, respectively.

In the experimental results of Fig.6(a) and Fig.8(a), a small corner separation can be found at the corner between the hub surface and the suction surface of the blade at ϕ=0.345 (ϕ_{design}). For low flow rate of ϕ=0.311 (0.9ϕ_{design}) in Fig.6(b) and Fig.8(b), and ϕ=0.276 (0.8ϕ_{design}) in Fig.6(c) and Fig.8(c), remarkable growth of separated region can be seen in the experiment.

Calculated results in Fig.7 and Fig.9 are compared with the experimental results as follows. Good qualitative agreement and fair quantitative agreement between the experiment and the calculation are obtained in such the points that a small corner separation is found at ϕ=0.345 (ϕ_{design}) and a remarkable growth of corner separation is seen at ϕ=0.276 (0.8ϕ_{design}).

On the other hand, at ϕ=0.311 (0.9ϕ_{design}), large separated region can be observed in the contour maps of the experiment of Fig.6(b) and Fig.8(b), whereas only small separated region can be found in the contour maps of the calculation of Fig.7(b) and Fig.9(b). This difference can be considered as follows. Numerical analysis is conducted under the assumption that flow is steady, therefore, no unsteady effect is included. Experimental results, however, have the periodical unsteady effect of rotor wake even though the experimental values are time-averaged. This difference can be considered as the reason of the difference between the experiment and the calculation atϕ=0.311 (0.9ϕ_{design}).

4.3 Streamlines in the Numerical Results

Figure 10, Fig.11 and Fig.12 show the limiting streamline patterns, where figures (a) show the limiting streamlines along the suction surface of the stator blade and figures (b) show the limiting streamlines along the hub surface. Fig.10, Fig.11 and Fig.12 show the flow field at ϕ=0.345 (ϕ_{design}), ϕ=0.311 (0.9 ϕ_{design}) and ϕ =0.276 (0.8 ϕ_{design}), respectively. In each figure, flow is from right to left, and LE and TE mean leading and trailing edge.

In Fig.10 at ϕ=0.345 (ϕ_{design}), the separation lines can be observed both on the blade suction surface and the hub surface, and very small separated region can be found on the hub surface. In Fig.11 at ϕ=0.311 (0.9 ϕ_{design}), the separation line on blade suction surface moves a little more upstream than the one at ϕ=0.345 (ϕ_{design}), and the separated region on the hub surface becomes a little wider than the one at ϕ=0.345 (ϕ_{design}).

In Fig.12 at ϕ =0.276 (0.8 ϕ_{design}), the separation line on the blade suction surface remarkably moves upstream especially near the hub, and the separated region on the hub surface becomes widespread largely. In the separated region on the blade surface, two foci can be observed, one is found at mid-chord and another is found at near the trailing edge. In the separated region on the hub surface, three foci can be observed at about 30% chord, 60% chord and at the rear of the trailing edge.

Figure 13 shows the streamlines issued from the hub surface and the suction surface at ϕ =0.276 (0.8 ϕ_{design}). Vortex behaviors in space can be observed in Fig.13, although the definite relation between the vortices which have legs on the blade suction side and the vortices which have legs on the hub surface. Near the trailing edge, it can be observed that vortices both from the blade suction surface and from the hub surface keep vortex structures up to far location from these wall surfaces.

4.4 Considerations of Vortical Flow

In order to consider the vortical flow field near the blade suction surface and the hub surface, the boundary layers near both surfaces are replaced by vortex filaments. Fig.14 shows the illustrations of a corner separation expressed by vortex filaments. Fig.14(a) shows the no-separated flow for the comparison. In the figure, flow is right to left, LE and TE mean leading and trailing edge, and a vortex filament is shown by a broken line and triangles. The vortical motion induced by a vortex filament is also shown. For the case of no-separated flow in Fig.14(a), the vortex filaments are considered to be attached to the both surfaces.

Figure 14(b) shows the separated flow without vortices. The separation lines on both surfaces are shown by one-dotted lines. In the figure, a separation of flow from the surface is interpreted as a separation of a vortex filament from the surface, which is one possible way of interpretation of a separated flow. In Fig.14(b), the vortex filaments near the trailing edge are separated from both the blade suction surface and the hub surface. At the cases of ϕ=0.345 (ϕ_{design}) and ϕ=0.311 (0.9 ϕ_{design}), the corner separation without vortices can be seen in Fig.10 and Fig.11, the vortical flow field for the cases can be explained by Fig.14(b).

Figure 14(c) shows the separated flow with vortices. A focus in a corner separation is shown by a solid circle. This flow model is a hypothetical model, which has an assumption that some of vortex filaments go into the separated region and are split.

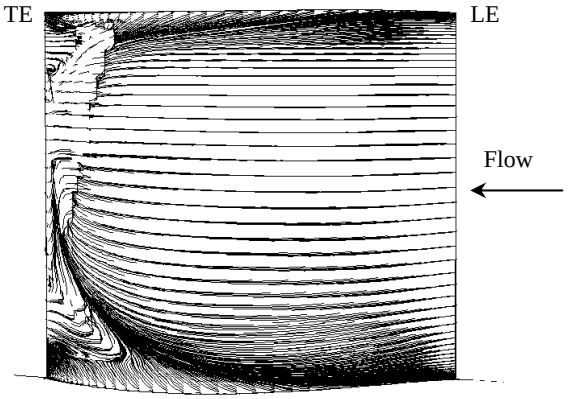

(a) Along the suction surface

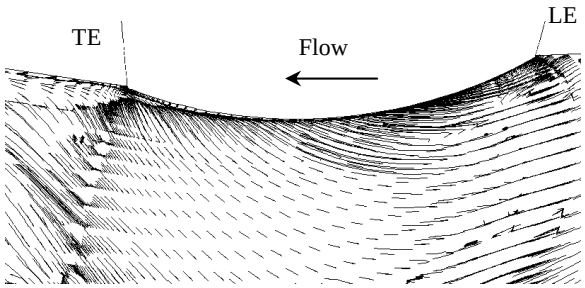

(b) Along the hub surface (suction surface side)

Fig. 10 Limiting streamlines at $\phi = 0.345$ (ϕ_{design})

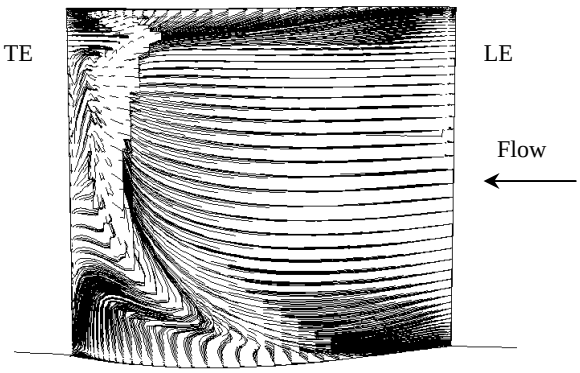

(a) Along the suction surface

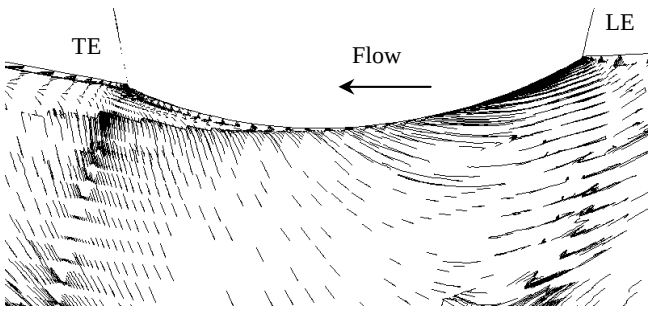

(b) Along the hub surface (suction surface side)

Fig. 11 Limiting streamlines at $\phi = 0.311$ ($0.9\phi_{design}$)

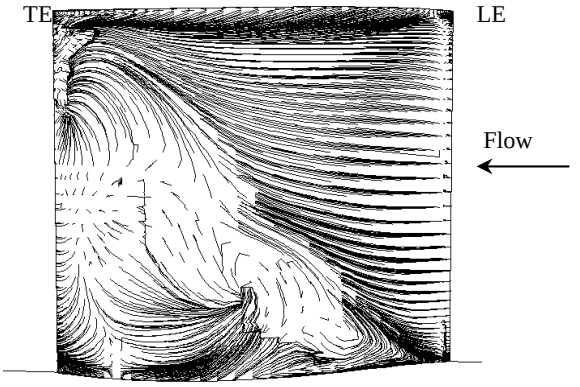

(a) Along the suction surface

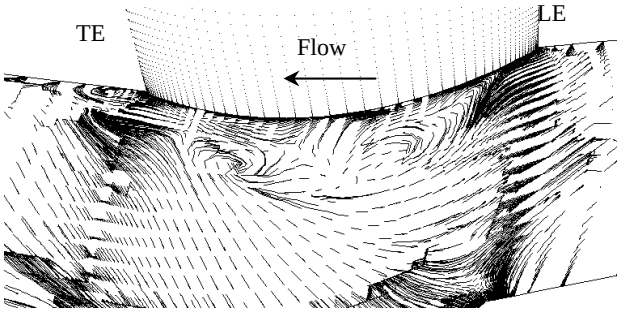

(b) Along the hub surface (suction surface side)

Fig. 12 Limiting streamlines at $\phi = 0.276$ ($0.8\phi_{design}$)

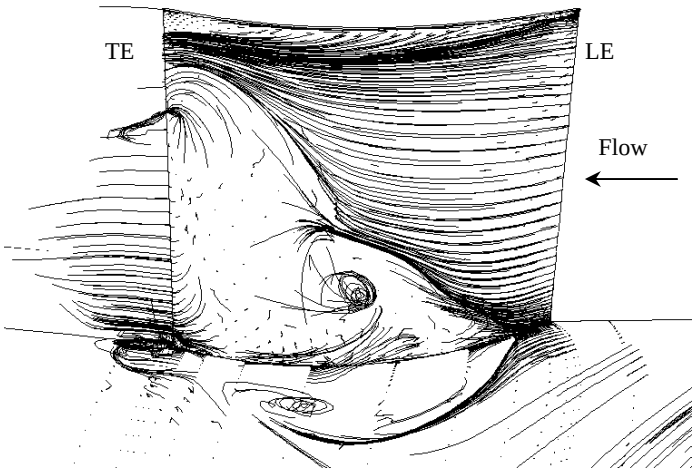

Fig. 13 Streamlines issued from hub and suction surface at $\phi = 0.276$ ($0.8\phi_{design}$)

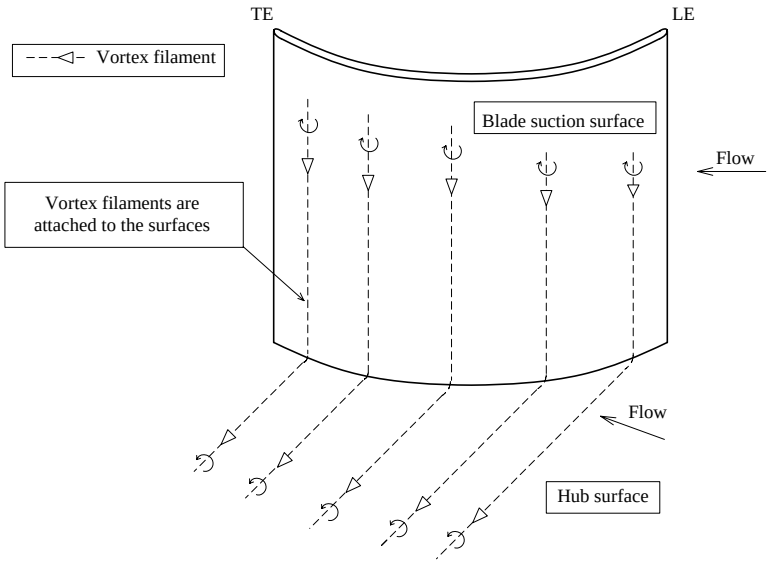

(a) no-separated flow

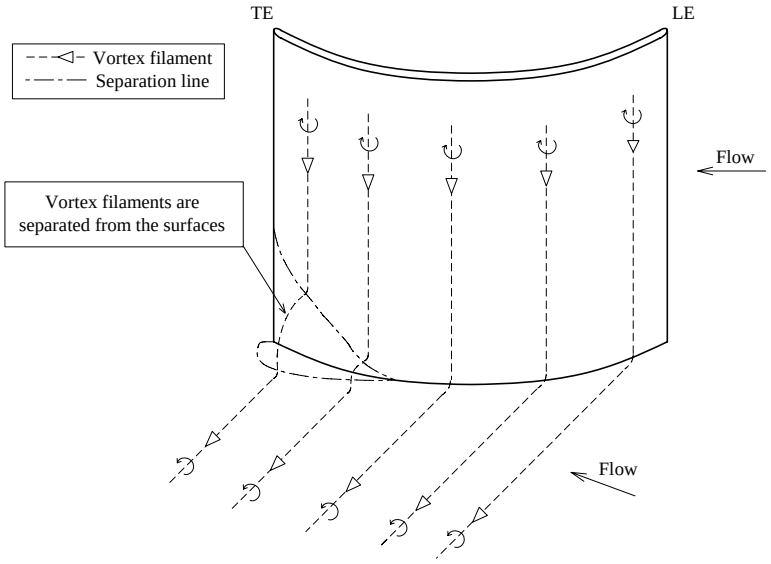

(b) separated flow without vortices

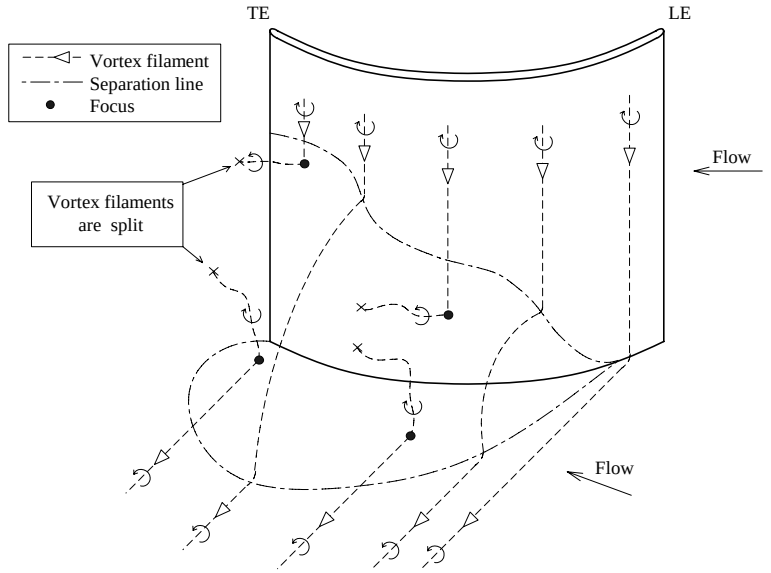

(c) separated flow with vortices

Fig. 14 Illustrations of a corner separation expressed by vortex filaments

If the assumption is allowed, the vortex filaments behave as foci and vortex cores within the separation region. Further investigation is needed to check the validity of this assumption. At the case of ϕ =0.276 (0.8 ϕ_{design}), a corner separation with vortices can be seen in Fig.12 and Fig.13, the vortical flow field for the case can be explained by Fig.14(c).

5. Conclusions

Experimental and numerical investigations were conducted for the internal flow in an axial flow stator of a diagonal flow fan. Corner separation near the hub surface and the suction surface of the stator blade are focused on, and further three-dimensional vortices in separated flow are investigated by the numerical analysis. Conclusions are summarized as follows.

(1) In the experiment, a small corner separation can be found at the corner between hub surface and suction of the stator blade at design flow rate. At 90% and 80% of design flow rate, remarkable growth of separated region can be seen in the experiment.

(2) Good qualitative agreement and fair quantitative agreement between the experiment and the calculation are obtained in such the points of a small corner separation at design flow rate and a remarkable growth of corner separation at 80% of design flow rate. The calculated separation region at 90% of design flow rate is smaller than the experimental one, the reason of this difference can be considered that the calculation assumes steady flow, whereas the experimental results include the periodical unsteady effect of rotor wake even though the experimental values are time-averaged.

(3) In the calculated results, the separation lines both on the blade suction surface and the hub surface move more upstream with decreasing the flow rate. At 80% of design flow rate, the hub corner separation becomes widespread remarkably and the foci can be observed in the separated region both along the blade suction surface and along the hub surface.

(4) At 80% of design flow rate, vortex behaviors in space can be observed, although the definite relation between the vortices which have legs on the hub surface and the vortices which have legs on the blade suction surface. Near the trailing edge, it can be observed that both vortices from the blade suction side and from the hub keep vortex structures up to far locations from these wall surfaces.

(5) In order to explain the vortices within the three-dimensional separation, the vortex filaments are used to express the boundary layers along both the blade suction surface and the hub surface. The vortices within the separation at 80% of design flow rate can be explained by the behavior of the vortex filaments provided that some of vortex filaments go into the separated region and are split.

Nomenclature

A	Reference area [m^2]	ϕ	Flow rate coefficient [-]
D_c	Casing diameter [m]	η	Total pressure efficiency [-]
D_h	Hub diameter [m]	ρ	Density of air [kg/m^3]
ΔP	Total pressure-rise [Pa]	τ	Torque coefficient [-]
P_t	Total pressure [Pa]	ω	Angular velocity [1/s]
Q	Volumetric flow rate [m^3/s]	ψ	Total pressure-rise coefficient [-]
r	Radius [m]		
T	Torque [Nm]		
U^*	Reference velocity [m/s]		
v_a	Axial velocity [m/s]		

References

[1] Joslyn H.D. and Dring R., 1985, “Axial Compressor Stator Aerodynamics,” ASME Journal of Engineering for Gas Turbines and Power Trans. ASME, Vol. 107, pp. 485-493.

[2] Dong Y., Gallimore S.J. and Hodoson H.P., 1987, “Three-Dimensional Flows and Loss Reduction in Axial Compressors,” Journal of Turbomachinery Trans. ASME, Vol. 109, pp. 354-361.

[3] Schulz H.D. and Gallus H.D., 1988, “Experimental Investigation of the Three-Dimensional Flow in Annular Compressor Cascade,” Journal of Turbomachinery Trans. ASME, Vol. 110, pp. 467-478.

[4] Hah C. and Loellbach J., 1999, “Development of Hub Corner Stall and Its Influence on the Performance of Axial Compressor Blade Rows,” Journal of Turbomachinery Trans. ASME, Vol. 121, pp. 67-77.

[5] Gbadebo S.A., Cumpsty N.A. and Hynes T.P., 2005, “Three-Dimensional Separations in Axial Compressors,” Journal of Turbomachinery Trans. ASME, Vol. 127, pp. 331-339.

[6] Kinoue, Y., Shiomi, N., Setoguchi, T. and Jin, Y., 2009, “Experimental Investigation on Separated Flows of Axial Flow Stator and Diagonal Flow Rotor,” International Journal of Fluid Machinery and Systems, Vol. 2, pp. 223-231.